

NOIRCAT – The Northern HIPASS Optical/IR Catalogue

O. I. Wong,^{1,2,3} R. L. Webster,¹ V. A. Kilborn,⁴ M. Waugh,¹ and L. Staveley-Smith⁵

¹*School of Physics, University of Melbourne, VIC 3010, Australia*

²*Australia Telescope National Facility, CSIRO, PO Box 76, Epping, NSW 1710, Australia*

³*Department of Astronomy, Yale University, New Haven, CT 06520-8101, USA*

⁴*Centre for Astrophysics & Supercomputing, Swinburne University of Technology, P.O. Box 218, Hawthorn, VIC 3122, Australia*

⁵*School of Physics, University of Western Australia, 35 Stirling Hwy, Crawley, WA 6009, Australia*

Accepted ***. Received ***; in original form ***

ABSTRACT

We present the Northern HIPASS Optical/InfraRed CATalogue (NOIRCAT), an optical/near-infrared counterpart to the Northern HIPASS catalogue (NHICAT). Of the 1002 sources in NHICAT, 655 (66%) have optical counterparts with matching optical velocities. A further 85 (8%) sources have optical counterparts with matching velocities from previous radio emission-line surveys. We find a correlation between the gas and stellar content of the NOIRCAT sources. Our H I-selected sample of isolated galaxies also present a wider range in near-infrared (NIR) colours than previous optically-selected studies of regular, isolated galaxies. All H I detections in optically unobscured fields could be matched with either a NED optical counterpart, or a galaxy visible in POSSII or DSS images. However, as over 200 of these matched galaxies have no velocity information, further follow-up observations are needed to confirm the matches, and hence confirm or deny the existence of dark galaxies in this dataset.

Key words: methods: observational - surveys - catalogues - radio lines: galaxies

1 INTRODUCTION

Primordial gas clouds are postulated to exist in the Local Universe due to the slow collapse of material about small density perturbations present in the matter density field (after the epoch of recombination) which have not reached the threshold density needed to form stars (Giovanelli & Haynes 1989). *N*-body simulations of galaxy formation using the Cold Dark Matter cosmological model (Moore et al. 1999; Klypin et al. 1999) predicted a significant number of small dark matter halos. Since dark matter halos exist around most galaxies, small dark matter haloes are assumed to exist around dwarf galaxies. However, current observations find the number of dwarf galaxies to be significantly less than the predicted number of small dark matter halos. Without modifying the large-scale properties of these models, it may be possible for small dark matter halos to exist and galaxies not to have been observed if star formation had been suppressed in these dark halos. Two possibilities exist: (i) the halos may contain gas but star formation is suppressed; (ii) the halos do not contain gas. Current reionisation models of the Universe predict the latter as they find that the gas from 95% of the low-mass systems ($M_{\text{virial}} \leq 10^8 M_{\odot}$ or $v_{\text{circ}} \leq 20 \text{ km s}^{-1}$) appears to have been photoevaporated during the epoch of reionisation (Susa & Umemura 2004).

Schneider (1996) suggested that H I surveys can be used to probe the regions of the Local Universe where stars have not formed since most surveys conducted with optical telescopes are biased against objects such as low surface brightness (LSB) galaxies and the proposed dark galaxies. There are also numerous objects such as NGC 2915, a small blue compact dwarf galaxy in optical wavelengths, with an enormous envelope of H I extending beyond 5 Holmberg radii (Meurer et al. 1996). Hence, blind all-sky H I surveys (i.e. HIPASS) may reveal a large undiscovered population of gas-rich LSB galaxies (Disney 1976) as well as other gas-rich dwarf galaxies.

The H I Parkes All-Sky Survey (HIPASS) is the largest blind H I survey, covering 71% of the total sky using the Parkes Radio Telescope¹. Northern HIPASS surveys the entire sky within the declination range $+2^{\circ} < \delta < +25.5^{\circ}$, whereas Southern HIPASS covers the entire Southern sky south of a declination of $+2^{\circ}$. The Northern HIPASS catalogue (NHICAT; Wong et al. 2006) and the Southern HIPASS catalogue (HICAT; Meyer et al. 2004) detected 1002 and 4315 galaxies respectively, based solely on the H I content. Here, we present the Northern HIPASS optical and

¹ The Parkes telescope is part of the Australia Telescope which is funded by the Commonwealth of Australia for operation as a National Facility managed by CSIRO.

near-**IR** catalogue (NOIRCAT)—a catalogue of optical and near-infrared counterparts to the HI galaxies in NHICAT. NOIRCAT is analogous to the HIPASS Optical Catalogue (HOPCAT; Doyle et al. 2005) which is a catalogue of optical counterparts for HICAT.

There are many theoretical arguments for (Davies et al. 2006; Verde et al. 2002) and against (Taylor & Webster 2005) the existence of dark galaxies which will be further discussed in Section 3. To avoid confusion, we define a dark galaxy to be an optically dark, isolated HI source, with no neighbouring galaxies and no stars. Previous discoveries of “dark” galaxies were either high velocity clouds (Kilborn et al. 2000) or gas clouds associated with optical galaxies (Schneider et al. 1983; Ryder et al. 2001). One of the best dark galaxy candidate is the isolated HI cloud, HI1225+02 (Giovanelli & Haynes 1989). Higher spatial resolution mapping of HI1225+01 showed two dynamically-distinct components (Chengalur et al. 1995); one of which is associated with a LSB dwarf, while the other (south-western cloud) is starless down to at least 27.2 magnitudes in the *I*-band (Turner & MacFadyen 1997).

The most recent unconfirmed dark galaxy candidate is GEMS_N3783_2, an isolated region of HI gas with no visible optical counterpart located within the NGC 3783 galaxy group (Kilborn et al. 2006). Kilborn et al. (2006) concluded that GEMS_N3783_2 was formed during the interaction of NGC 3706 and ESO 378-G003. However, the projected separation of GEMS_N3783_2 and ESO 378-G003 is 450 kpc with no obvious HI bridge or tail structures. Hence deeper follow-up observations are needed to confirm and uncover any further HI or optically-faint counterparts remaining in this system.

Previous blind HI surveys, including HIPASS, have not found any evidence for the existence of dark galaxies. Even though the main purpose of NOIRCAT is to provide complementary optical/near-infrared data to NHICAT, NOIRCAT will also be able to provide an independent search for dark galaxies.

Section 2 describes the construction of NOIRCAT and the properties of the catalogued galaxies. Discussion of the scientific implications can be found in Section 3 and Section 4 provides a summary of our results.

2 NOIRCAT

This section describes the method used to produce NOIRCAT and the properties of NOIRCAT. To probe the existence of dark galaxies, sources with no optical velocity matches within $7.5'$ of the HIPASS centre will be further analysed in Section 2.3.

2.1 The construction of NOIRCAT

There have been several methods with which catalogues of optical counterparts of HIPASS samples have been produced. Both Kilborn et al. (2002) and Ryan-Weber et al. (2002) used NED² to search for known optical counterparts to each of the HI sources in the South Celestial

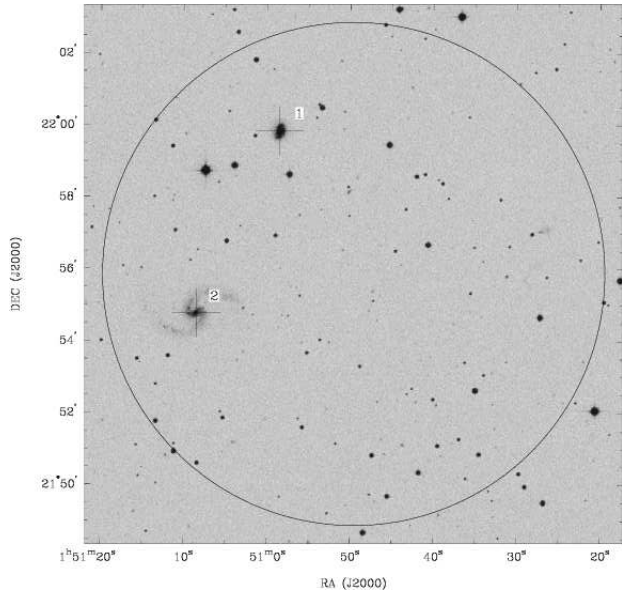


Figure 1. Screenshot of an example field window used during the interactive inspection. The field centre is of HIPASSJ0150+21, a Flag 3 detection. The circle shows the $7.5'$ radius from the HIPASS centre which is in the centre of the field. All matches found in NED are marked by a ‘+’ and a number corresponding to an optical source listed in the text window.

Cap (SCC) sample and the HIPASS Bright Galaxy Catalogue (BGC; Koribalski et al. 2004), respectively. On the other hand, HOPCAT was produced using an automated visual interactive program which displays SEXTRACTOR (Bertin & Arnouts 1996) ellipses representing areas within the SUPERCOSMOS fields which are above the sky intensity as well as velocities derived from both 6dF and NED. The automated visual display program was then used by three people to interactively compile HOPCAT. In HOPCAT, an optical match is proposed when the HIPASS velocity is within 400 km s^{-1} of the velocity derived from NED/6dF and the positional match is within the $15' \times 15'$ SUPERCOSMOS field.

The large Southern sky surveys used to generate HOPCAT, such as 6dF and SUPERCOSMOS, are not available for the construction of NOIRCAT. Northern analogues of 6dF and SUPERCOSMOS do not exist. Most large, recent optical surveys such as SDSS do not cover the entire Northern sky. Hence, NED is used as our source catalogue for optically matching the Northern HIPASS detections. It should be noted that we used the October 2006 version of NED. To improve optical detection limits, we also used the 2MASS near-infrared catalogue. For NOIRCAT, the primary method for determining the optical/near-infrared matches was by “interactive” cataloguing, after an automated search of the NED and 2MASS catalogues. The automated search identified all the NED and 2MASS sources within $7.5'$ and 400 km s^{-1} of each NHICAT source. These preliminary search criteria were intended to be simple, in order to include galaxies that may have extended HI, or

² The NASA/IPAC Extragalactic Database (NED) is operated by the Jet Propulsion Laboratory, California Institute of Tech-

nology, under contract with the National Aeronautics and Space Administration.

Table 1. Definition of flags in the processing of NOIRCAT and the total number of Northern HIPASS sources within each flag category.

Flag	Definition	Total
1	Single optical velocity match with 2MASS counterpart	414
2	Single optical velocity match without 2MASS counterpart	126
3	Multiple optical velocity matches where all matches also have 2MASS counterparts	63
4	Multiple optical velocity matches where one or more matches are without 2MASS counterparts	52
5a	No optical velocity match but with higher angular resolution HI velocity match	85
5b	No velocity match but positional matches available to NED galaxies	221
5c	No velocity or positional matches to any galaxies listed in NED	41

an HI distribution that is offset from the optical counterpart. These parameters are also consistent with HOPCAT’s matching criteria.

The preliminary matches were then plotted with a ‘+’ and a number onto an optical field centred on the corresponding HIPASS source centre. Figure 1 shows an example of the graphics window shown for HIPASSJ0150+21 (a Flag 3 source) during this interactive process. Each HIPASS field is displayed (with a list of properties found from the automated search), inspected and graded using the interactive process. The list of properties displayed include the HIPASS velocity, velocity width, name, optical velocities (and errors) as well as the availability of 2MASS magnitudes for each of the NED sources found. We obtained optical fields for all the NHICAT sources from the Second Palomar Sky Survey (POSSII; Reid et al. 1991) in the red band. Table 1 shows the five main categories into which each source was sorted.

During the interactive process, the appropriate optical matches and match category are determined for each HIPASS source. The three rules used for determining a match are:

- (i) Optical sources must be within $7.5'$ of the HIPASS centre. Where there are multiple source names referring to the same source (e.g. SDSS and APM nomenclatures), the non-SDSS/APM reference is preferred.
- (ii) Optical velocity matches are made when the published optical velocity (including velocity uncertainties) is consistent to within 100 km s^{-1} of the HIPASS velocity profile.
- (iii) For optical velocities without published errors in NED, a match is recorded when the published optical velocity is within 150 km s^{-1} of the HIPASS velocity profile.

To be consistent with previous HIPASS optical counterpart catalogues (Ryan-Weber et al. 2002; Doyle et al. 2005), we chose $7.5'$ to be the maximum angular separation between a HIPASS source centre and potential optical match. Although the predicted position accuracy is $\sim 3'$, the position accuracy also depends on the HI peak flux density, the source extent and any asymmetries or confusion intrinsic to the source (Barnes et al. 2001). Previous catalogues have also found match separations greater than $5'$. Within HOPCAT, 0.6% (~ 25 sources) of the HIPASS-optical velocity matches correspond to angular separations greater than $7.5'$ even though the average HIPASS beam FWHM is $14.3'$ (Barnes et al. 2001). Other reasons for positional matches beyond $\sim 3'$ will be further discussed in Section 3.

The interactive cataloguing was undertaken by two in-

dependent researchers (Wong and Waugh). It should be noted that, unlike HOPCAT, all multiple optical matches (Flag 3 or 4) will be listed in NOIRCAT and no attempt has been made to choose between possible matches. In these cases, discrimination can only be made with higher angular and velocity resolution HI observations.

2.2 Properties of NOIRCAT

We found that 655 of 1002 NHICAT sources could be matched with previously-catalogued galaxies for which an optical velocity was available (Flags 1 to 4). Of these 655 sources, 82% are matches to single galaxies and of these matches, 73% have 2MASS observations in the J , H and K wavebands. Table 1 summarises the distribution of NHICAT sources over the seven match categories. A full description of NOIRCAT’s parameters and an example of the first 10 sources in NOIRCAT can be found in Table 2. The total NIR J , H and K magnitudes from 2MASS are also listed in NOIRCAT. Corrections³ were made to account for the 10%–20% flux loss due to the very high background levels in the 2MASS observations.

To examine the properties of these matched galaxies, we use the 2MASS J , H and K magnitudes instead of the optical magnitudes because the 2MASS catalogue is the best available optical/NIR catalogue and has the best Northern sky coverage corresponding to the sky coverage of Northern HIPASS. The NIR wavelengths are also less sensitive to the dust obscuration in the Galactic plane. The NIR apparent magnitudes can be used as stellar mass indicators. The NIR observations are better tracers of mass distribution because NIR emission is derived primarily from cooler giant and dwarf stars (instead of hot young stars) which account for a major fraction of the bolometric luminosity of a galaxy. Using the NIR observations, we explore the relationships between the HI content of HIPASS galaxies and their inferred stellar content.

Figure 2 shows the HI absolute magnitude⁴ ($M_{21\text{cm}}$) of Flag 1 sources as a function of the J , H and K absolute magnitudes. The flux observation limit of Northern HIPASS is 0.07 Jy for a detection that is 5 times the RMS.

³ More details on the 2MASS processing can be found at: http://www.ipac.caltech.edu/2mass/releases/allsky/doc/sec4_5e.html#large

⁴ The HI absolute magnitude has been calculated using the AB magnitude system via: $m = -2.5 \log(f) - 48.6$ where f is the measured HI flux in units of $\text{ergs s}^{-1} \text{ cm}^{-2} \text{ Hz}^{-1}$

Table 2. Example of the first 10 sources of NOIRCAT. The parameters are further described below the table. It should be noted that Flag 5b and 5c sources will not be listed in NOIRCAT.

(1) HIPASS_name	(2) RA_HIPASS	(3) Dec_HIPASS	(4) Vel_HIPASS	(5) W_HIPASS	(6) Flag	(7) Optical_source	(8) RA_Optical
	(9) Dec_optical	(10) Separation	(11) NED_type	(12) NED_morph	(13) Vel_optical	(14) Vel_err_optical	(15) Vel_source
	(16) J	(17) J_err	(18) H	(19) H_err	(20) K	(21) K_err	
HIPASSJ0001+05	00:01:39.0 +05:23:22	05:18:47 5.3	3956.9 Galaxy	48.2 SB(r)m	5 3949	UGC12910 5	00:01:28.4 1990ApJS...72..245S
HIPASSJ0002+16a	00:02:08.4 +16:35:25	16:35:13 0.7	1047.3 Galaxy	108.5 Im	5 1050	IC 5377 4	00:02:05.4 1990ApJS...72..245S
HIPASSJ0002+16b	00:02:54.9 +16:08:44 8.089	16:08:51 4.8 0.020	1047.1 Galaxy 7.361	456.8 SA(S)ab 0.023	1 1050 7.084	NGC 7814 4 0.024	00:03:14.9 1999ApJS..121..287H
HIPASSJ0003+07	00:03:46.1 +07:28:43 10.561	07:29:02 0.8 0.024	5240.5 Galaxy 9.863	181.9 Sbc 0.030	1 5241 9.525	NGC 7816 5 0.034	00:03:48.8 1999ApJS..121..287H
HIPASSJ0003+15	00:03:58.4 +15:13:06	15:11:59 3.8	873.8 Galaxy	100.6 Sm	5 878	UGC00017 6	00:03:43.3 1991RC3.9.C...0000d
HIPASSJ0004+07	00:04:17.6 +07:22:46 12.117	07:21:47 2.4 0.046	6193.1 Galaxy 11.499	198.7 Scd 0.066	1 6201 11.079	NGC 7818 1 0.069	00:04:08.8 1999ApJS..121..287H
HIPASSJ0004+20	00:04:18.1 +20:45:08 9.489	20:49:39 6.4 0.006	2162.1 Galaxy 8.734	107.1 SAbc 0.007	1 2310 8.421	NGC 7817 1 0.008	00:03:58.9 1999ApJS..121..287H
HIPASSJ0004+05	00:04:34.4 +05:50:50 13.275	05:50:00 1.6 0.076	3112.2 Galaxy 12.749	221.0 Scd 0.120	1 3118 12.265	UGC00027 1 0.131	00:04:28.8 1999ApJS..121..287H
HIPASSJ0006+17	00:06:30.3 +17:17:03	17:20:22 3.8	875.4 Galaxy	78.4 Sdm	5 873	UGC00047 4	00:06:38.3 1990ApJS...72..245S
HIPASSJ0006+08	00:06:45.7 +08:37:43 11.361	08:37:26 1.0 0.037	5255.2 Galaxy 10.772	210.5 SAc 0.053	1 5257 10.405	UGC00052 2 0.060	00:06:49.5 1999ApJS..121..287H

NOTE.— Parameter definitions. (1): HIPASS identification. (2): HIPASS right ascension (J2000). (3): HIPASS declination (J2000). (4): HIPASS heliocentric velocity at FWHM (km s^{-1}). (5): HIPASS velocity width (km s^{-1}). (6): Optical match category flag. (7): Source name of optical match. (8): Right ascension (J2000) of optical source. (9): Declination (J2000) of optical source. (10): Spatial separation between the HIPASS source centre and the matched source ('). (11): NED's classification of source type (e.g. Galaxy, Galaxy Pair). (12): Published NED morphology. (13): Velocity of optical source (km s^{-1}). (14): Velocity error of optical source (km s^{-1}). (15): Reference for optical velocity. (16): *J*-band magnitude from total 2MASS flux. (17): *J*-band magnitude error from 2MASS. (18): *H*-band magnitude from total 2MASS flux. (19): *H*-band magnitude error from 2MASS. (20): *K*-band magnitude from total 2MASS flux. (21): *K*-band magnitude error from 2MASS.

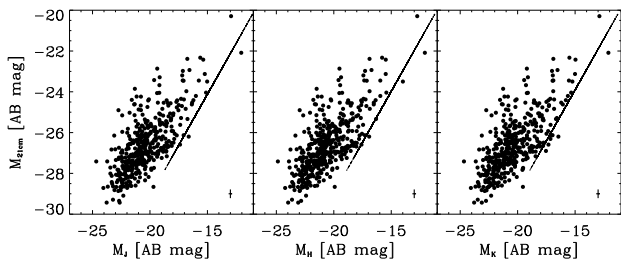


Figure 2. HIPASS absolute magnitude ($M_{21\text{cm}}$) as a function of J , H and K absolute magnitudes for the 414 Flag 1 sources. The solid line in each plot shows the combined HIPASS limit for a detection that is five times the RMS and a 2MASS detection with a SNR of 10. The average uncertainty for our data is shown by the error bar at the bottom right corner of each plot.

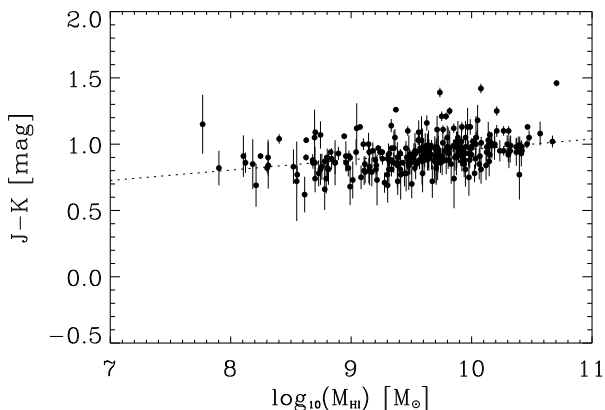


Figure 3. $J - K$ colour as a function of HI mass for the Flag 1 sources with reliable 2MASS colours. The dotted line shows the best robust linear fit to the data.

Likewise, the 2MASS observation limits are at $\log_{10}(J) = -19.0 \text{ W cm}^{-2} \mu\text{m}^{-1}$, $\log_{10}(H) = -19.2 \text{ W cm}^{-2} \mu\text{m}^{-1}$ and $\log_{10}(K) = -19.4$ for a $SNR = 10$ detection in the J , H and K bands, respectively. A Pearson correlation test resulted in an R -value of 0.72 for the relationship between all three NIR magnitudes with respect to $M_{21\text{cm}}$. This correlation at a 99.9% confidence level suggests that galaxies with more luminous in the NIR also have more HI. However, it should be noted that this correlation may be highly biased by the detection limits of the samples used and that at any given HI mass, there exists a broad range in NIR luminosity (as shown in Figure 2).

Bell & de Jong (2001) found a correlation between the stellar mass-to-light ratios and the colours of galaxies from the 2MASS/SDSS passbands. Using the NIR colours, we can distinguish between the galaxies which consist mainly of young stars, from the galaxies with larger fractions of older giants. The derived total NIR fluxes in 2MASS are too sensitive to stellar contamination and irregularities in

the surface brightness profiles⁵ for the determination of NIR colours. Therefore, to study the NIR colour properties of our sample, we use the NIR magnitudes from the 2MASS isophotal photometry. More accurate NIR colours are obtained, even though these flux values do not reflect the total flux of a source since the isophotal measurements are set at the 20th magnitude per arcsecond squared at the K_s band (which roughly correspond to 1σ of the background RMS). Figure 3 shows the $J - K$ colours (of 264 Flag 1 sources with reliable 2MASS isophotal photometry in all three J , H and K bands) as a function of the HI mass (M_{HI}). Following Roberts (1962), the HI mass was calculated from:

$$M_{\text{HI}} = 2.356 \times 10^5 D^2 \int S dv, \quad (1)$$

where Hubble Flow distances (D) assuming $H_0 = 73 \text{ km s}^{-1} \text{ Mpc}^{-1}$ and HI integrated fluxes ($\int S dv$) are used. We found the best linear fit to be $J - K = 0.08 \log(M_{\text{HI}}) + 0.18$. Most of the observed scatter can be attributed to the uncertainties from the 2MASS automated processing pipeline (Jarrett 2007). A good correlation was found between the HI mass and the NIR $J - K$ colours (Pearson R -value = 0.37), which suggests that galaxies with greater HI masses appear to have redder $J - K$ colours at a 99.9% confidence level. This agrees with previous work (e.g. Hanish et al. 2006) which found that galaxies with greater HI mass correspond to galaxies with greater optical R -band luminosity densities. Our results are also complementary to the findings of Bell et al. (2003) that galaxies with redder optical colours have greater mass-to-light ratios.

Near-infrared studies of normal non-interacting galaxies with nuclei dominated by older stars found that such galaxies span a very narrow window in the $J - H$ versus $H - K$ colour-colour diagram (Geller et al. 2006; Giuricin et al. 1993). Currently, the largest sample of NIR colours of galaxy pairs is catalogued by Geller et al. (2006). The NIR properties of these interacting galaxies were compared to the NIR properties of normal galaxy population from the Nearby Field Galaxy Sample, NFGS (Jansen et al. 2000a,b). A broader distribution of $J - H$ and $H - K$ colours were found for these interacting galaxies than for average field galaxies. Geller et al. (2006) interpreted this result as evidence for bursts of star formation (which shifts the NIR colours blueward) and for a dust-reddened/extincted and/or radiation from hot dust (which in turn results in redder colours). Radiation from hot dust is thought to be responsible for the reddest $H - K$ colours.

Our HI-selected sample of galaxies provides an interesting comparison to these previous NIR studies based on optically-selected samples. Figure 4 shows a NIR colour-colour plot of the same sources as in Figure 3. The points from our dataset are plotted in grey where 95% of our sources lie within the colour distribution marked by the black solid contour. Also plotted on Figure 4 is a black cross indicating the range of NIR colours for normal galaxies (Geller et al. 2006; Giuricin et al. 1993). The region enclosed by the dotted-lines mark the range of NIR colours found from the NFGS used by Geller et al. (2006) as the benchmark of a normal field galaxy sample.

⁵ http://www.ipac.caltech.edu/2mass/releases/allsky/doc/sec2_3b.html

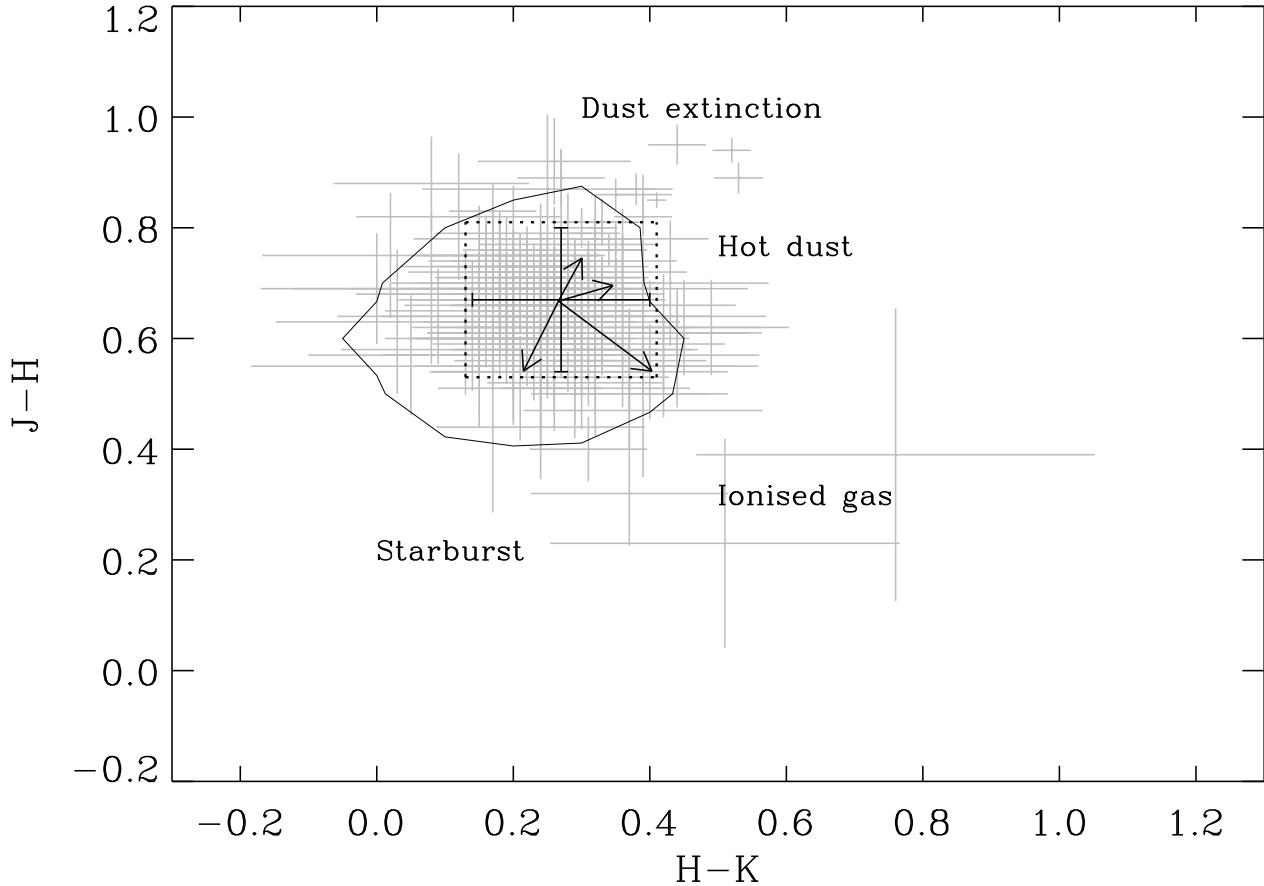


Figure 4. $J - H$ versus $H - K$ colour-colour diagram for the Flag 1 sources with reliable 2MASS colours (in grey). The black contours provide the $2\text{-}\sigma$ contour of the two-dimensional NIR colour distribution of our sample. The black cross marks the normal range of NIR colours (indicated by the error bars) for galaxies with nuclei dominated by an older stellar population. The black arrows indicate the shift in direction of a galaxy’s NIR colours due to factors such as starburst events, gaseous emission from ionised regions, thermal re-radiation of hot dust and reddening (Geller et al. 2006).

A simple model was proposed by Geller et al. (2006) to explain qualitatively the distribution of colours observed between the sample of galaxy pairs and the NFGS sample. Their model explained that: (i) dust extinction will redden the intrinsic colour of the galaxies, (ii) emission from bursts of star formation will shift the NIR colours blueward, (iii) re-radiation from hot dust will in general redden the NIR colours, particularly the $H - K$ colours, and (iv) the emission from regions with ionised gas shifts the $J - H$ colours blueward and the $H - K$ colours redward. These effects are summed up in Figure 4 as vector arrows extending away from the median NIR colour of the normal field galaxies.

As can be seen from Figure 4, our dataset is not entirely concentrated within the NIR colour region for the normal galaxies found by Geller et al. (2006) and Giuricin et al. (1993). In total, 41 galaxies (15.5%) of our sample have NIR colours outside the region bounded by the dotted lines in Figure 4. Of the outlying galaxies, 18 galaxies (6.8%) have $J - H < 0.54$ which suggests the existence of galaxies within our HI-selected sample that exhibit the effects of

star formation and gaseous ionising regions which appear proportionally under-sampled by the optically-based NFGS sample. Although bursts of star formation may be responsible for shifting the $H - K$ colours bluewards, it is not clear why 6 galaxies (2.3%) of our sample are found to have $H - K < 0.14$ and $J - H > 0.67$. No physical mechanism appear to be able to shift the $H - K$ colours blueward and the $J - H$ colours redward simultaneously.

We attribute these unusual NIR colours to the large uncertainties inherent in the measured isophotal magnitudes due to the high background levels of the 2MASS observations. Five of the six galaxies have very low surface brightnesses (with J -band magnitudes between 13.0 and 14.9), while the remaining source appears to have a very variable background level. The 2MASS photometry pipeline is susceptible to deriving unphysical NIR colours in galaxies due to contamination by foreground stars and variable background gradients⁵.

Table 3. NHICAT properties of 25 Flag 5b sources found with probable matches to sources not listed in NED.

HIPASS_name	RA_HIPASS (J2000)	Dec_HIPASS (J2000)	Vel_HIPASS (km s ⁻¹)	W_HIPASS (km s ⁻¹)	Galactic Latitude (°)
HIPASSJ0050+08	00:50:06.4	08:37:51	9972.0	124.1	-54.24
HIPASSJ0358+10	03:58:36.1	10:03:19	1978.0	141.2	-31.36
HIPASSJ0413+21	04:13:53.3	21:00:08	3630.8	150.3	-21.33
HIPASSJ0426+18	04:26:41.1	18:29:16	3974.9	64.7	-20.72
HIPASSJ0443+14	04:43:54.9	14:19:57	2726.3	35.9	-20.03
HIPASSJ0703+03	07:03:06.6	03:10:47	3548.8	103.4	4.04
HIPASSJ0727+04	07:27:39.6	04:40:51	2087.0	120.9	10.18
HIPASSJ0758+10	07:58:12.7	10:59:36	2346.0	94.5	19.75
HIPASSJ0821+03b	08:21:45.9	03:21:04	4132.7	252.8	21.58
HIPASSJ0835+14	08:35:15.8	14:15:07	5899.2	176.7	29.33
HIPASSJ0836+05	08:36:37.5	05:14:54	1865.6	60.4	25.74
HIPASSJ1025+20	10:25:29.9	20:14:24	1209.4	59.6	56.01
HIPASSJ1048+12a	10:48:00.8	12:13:37	955.2	136.8	57.49
HIPASSJ1154+12	11:54:16.0	12:26:29	1004.6	47.9	70.12
HIPASSJ1327+19	13:27:14.3	19:51:31	7152.4	115.0	79.04
HIPASSJ1515+05	15:15:18.5	05:50:20	677.7	93.1	49.73
HIPASSJ1551+08	15:51:41.2	08:01:23	5121.2	52.1	43.32
HIPASSJ1917+11	19:17:24.0	11:53:13	4542.4	38.3	-0.26
HIPASSJ1919+14	19:19:44.4	14:05:44	2811.9	169.0	0.27
HIPASSJ1922+18	19:22:50.1	18:42:50	3934.7	336.1	1.79
HIPASSJ1937+09	19:37:31.1	09:21:00	3148.2	81.0	61.23
HIPASSJ1949+24	19:49:58.4	24:10:50	3111.1	253.6	-1.05
HIPASSJ2306+14	23:06:07.3	14:43:10	1556.4	109.0	-40.97
HIPASSJ2316+15	23:16:54.1	15:47:44	4491.4	78.5	-41.33
HIPASSJ2347+06	23:47:25.0	06:47:59	3273.2	87.6	-52.70

The masking of nearby foreground stars can be incomplete or not performed in some galaxies and therefore the resultant photometry for the galaxy will be corrupted. Airglow gradients (from atmospheric OH airglow emission) in the background levels affect the accuracy of the measured photometry. This airglow noise is known to vary strongly with time, spatial position and the size and total brightness of the extended source. In the *H*-band, the additional uncertainty introduced by airglow is approximately equivalent to the measurement error⁶.

Therefore, the NIR colours of our HI-selected sample of galaxies appear largely consistent with the NIR colours of the NFGS sample. We attribute most of the observed scatter in NIR colours within our sample to the uncertainties in the 2MASS photometry. Our sample may also include a greater fraction of star-forming galaxies exhibiting the effects of star formation and ionised gas than the NFGS sample.

2.3 The search for dark galaxies

For the 35% of NOIRCAT sources without optical velocity matches (Flag 5), we attempt to match these sources to sources from previous HI surveys observed with a smaller spatial beamwidth than 7 arcminutes. For example, observations from the Very Large Array (VLA) with typical beam-sizes below an arcminute will provide a suitable sample with which to compare. The combination of a more accurate pointing and the velocity of the HI emission allow us to pinpoint the exact galaxy from which the emission is observed. Using the same interactive software algorithm detailed in Section 2.1, we classify 87 optically-visible galaxies found with matching HI velocities as Flag 5a sources (see Table 1).

Of the remaining 260 Flag 5 sources, 219 have one or more positional matches with galaxies listed in NED (see Appendix A). We identified these sources to be Flag 5b sources, and the rest of the sources (with no matches within 7.5' to galaxies in NED) were catalogued as Flag 5c sources. We found 25 Flag 5c sources with possible positional matches to galaxies observed in the POSSII/DSS fields but not listed in NED (see Table 3). The remaining 16 Flag 5c sources for which there were no optically-visible galaxies in the POSSII fields are listed in Table 4. One of the sources (HIPASSJ0843+21) has a bright foreground star saturating the field, while the other 15 are located in crowded stellar fields in the direction of the Galactic plane. The mean Galactic latitude of these 15 sources is -0.97° .

A consistent result was found by Ryan-Weber et al. (2002), who found optical counterparts for their entire sample except for one HIPASS BGC source, which was located behind the Large Magellanic Cloud (LMC) where the field was too obscured for any identification. Figure 5 shows the Galactic latitude of the NHICAT sources as a function of their measured heliocentric velocity for different types of NOIRCAT matches. Evidently, the distribution of the NOIRCAT galaxies is dominated by the substructure of the Local Universe.

In summary, no dark galaxy candidate has been identified in NOIRCAT. Since there exists 244 galaxies for which a possible optical counterpart can be observed in the POSSII fields, follow-up higher spatial resolution observations with velocity information will pinpoint the exact location of the HI source. Although we currently cannot rule out the existence of dark galaxy within our sample, the likelihood of their existence is small.

3 DISCUSSION

In this section, we examine the effectiveness of our identification process and the reliability of NOIRCAT. Can we statistically estimate how many of our optical matches are due to random matches? We first determine the probability of identifying an optical source due to chance projection of positions on the sky by querying the NED database for 1,000 semi-random source positions chosen one degree away in angular separation (in a random direction) from any NHICAT source position in order to account for the structure and clustering of the Local Universe. Figure 6 presents the sample-normalised distributions of the NOIRCAT match separations (solid line) and those of the semi-random matches (dotted line) divided into three Galactic latitude ranges. The match separation distribution for the semi-random matches have a larger average match separation than the distribution observed for the NOIRCAT matches. It should be noted that only the Flag 1, 2 and 5a NOIRCAT sources are represented in the solid line distributions shown in Figure 6. The observed peaks in the middle panel of Figure 6 are due to the small sample size and are not real.

Assuming that the real match separation distribution does not have a tail and that all match separations greater than five arcminutes are random matches, we fit the tail-end (where match separations is greater than 5 arcminutes) of the NOIRCAT match separation distributions with a scaled-down distribution of the semi-random sample. From this, we can estimate a conservative upper limit on the possible number of random matches within NOIRCAT if the NOIRCAT matching algorithm was entirely based on the two-dimensional positions of the objects on the sky. Figure 7 shows this scaled model distribution of random matches as a grey line-filled distribution which has been scaled-down from the initial distribution of semi-random matches (shown in dotted lines). We find that 248 of the 408 matches in the Northern ($b \geq +5^\circ$) NOIRCAT distribution may be due to random matches. Similarly, 58 of 215 matches in the Southern ($b \leq -5^\circ$) NOIRCAT distribution may be due to random matches. Each NOIRCAT match along the Galactic equator ($-5^\circ < b < +5^\circ$) is real since the semi-random distribution is completely different to the observed distribution. Table 5 provides a summary these results. Therefore, the upper limit on the number of NOIRCAT matches resulting from a chance projected alignment on the sky (if our matching algorithm was based solely on the positions of the sources) is 48%.

However, 74% of NOIRCAT have matches in position as well as in velocity. The inclusion of velocity provides a better discriminant between real and spurious matches. Although we use a very loose $\pm 400 \text{ km s}^{-1}$ velocity offset to allow for

⁶ http://www.ipac.caltech.edu/2mass/releases/allsky/doc/sec1_6c.html#out

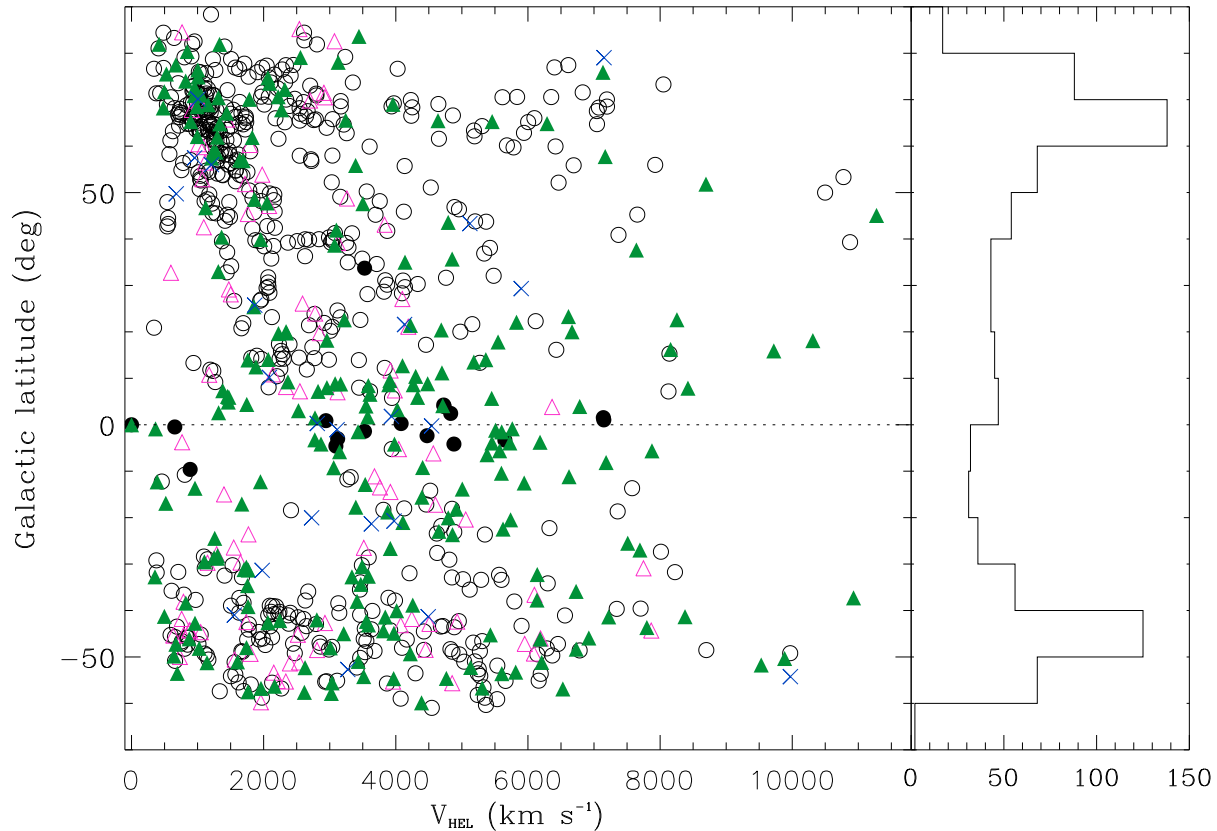


Figure 5. The galactic latitude of each match as a function of heliocentric velocity from NHICAT. The black open circles represent the NOIRCAT sources in Flags 1, 2, 3 and 4. The pink open triangles represent the 87 Flag 5a sources with previous HI velocity matches. The green solid triangles and the blue crosses represent the 219 Flag 5b sources (with probable matches based on positional matches) and the 25 category 5c sources (with probable matches with galaxies not listed in NED), respectively. The remaining 16 Flag 5c sources without any matches to optically-visible galaxies are represented by the black solid circles. The cluster of sources found at velocities of ~ 1000 km s $^{-1}$ and at Galactic latitude of 65° corresponds to the Virgo Cluster. The cluster of sources at Galactic latitude of -50° is a result of projection effects and is not the location of any known clusters. On the *right* panel, the distribution of Galactic latitude of all the NOIRCAT sources is shown.

Table 4. NHICAT properties of the 16 Flag 5c sources without optical counterparts.

HIPASS name	RA (J2000)	Dec (J2000)	Vel _{HEL} (km s $^{-1}$)	W (km s $^{-1}$)	Gal_Lat (deg)
HIPASSJ0542+11	05:42:43.6	11:27:29	887.3	109.4	-9.61
HIPASSJ0608+13	06:08:35.7	13:06:50	5650.8	66.2	-3.30
HIPASSJ0636+04	06:36:48.2	04:02:12	3526.1	191.0	-1.41
HIPASSJ0843+21 [†]	08:43:14.6	21:29:23	3527.6	146.1	33.72
HIPASSJ1853+09	18:53:58.0	09:51:52	4731.7	331.9	3.92
HIPASSJ1900+13	19:00:02.1	13:30:32	4724.8	96.7	4.25
HIPASSJ1901+06	19:01:35.4	06:52:00	2942.2	79.8	0.88
HIPASSJ1914+10	19:14:58.4	10:17:37	654.7	81.6	-0.47
HIPASSJ1919+18	19:19:53.7	18:47:37	4830.6	118.8	2.44
HIPASSJ1921+14	19:21:35.8	14:54:15	4080.3	81.7	0.25
HIPASSJ1922+08	19:22:10.4	08:13:21	3119.8	112.5	-3.01
HIPASSJ1927+20	19:27:31.5	20:13:41	7141.0	72.4	1.53
HIPASSJ1929+08	19:29:09.1	08:06:27	3092.7	225.6	-4.59
HIPASSJ1937+23	19:37:06.8	23:15:34	7148.5	161.7	1.04
HIPASSJ1942+18	19:42:45.1	18:40:58	4473.0	127.0	-2.36
HIPASSJ1950+18a	19:50:40.8	18:20:05	4879.6	152.2	-4.16

[†] This source has a foreground star saturating its optical field.

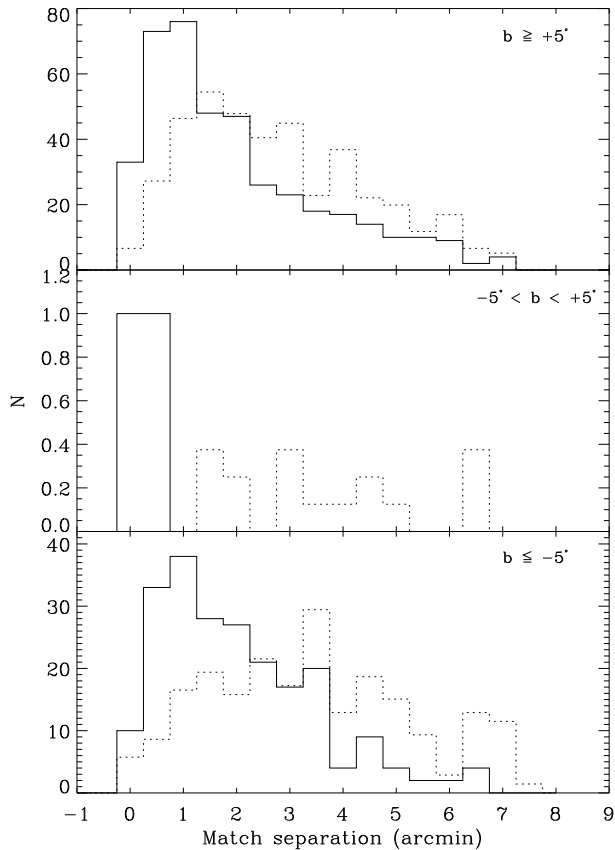


Figure 6. Distributions of match separations at three different Galactic latitude (b) ranges. The top, middle and bottom panels show the match separations for sources located at $b \geq +5^\circ$, $-5^\circ < b < +5^\circ$ and $b \leq -5^\circ$, respectively. The match separation distributions of the NOIRCAT matches (Flag 1, 2 & 5a) are represented by the solid histograms, while the dotted line histograms show the distributions for the simulated sources which are one degree away from any NHICAT source positions. It should be noted that the NOIRCAT sample had two sources in the range of $-5^\circ < b < +5^\circ$. In addition, the observed peaks in the simulated distribution in the middle panel is due to the smaller sample size.

possible matches, the average velocity difference (between the HIPASS and optical/IR velocities) is 22 km s^{-1} . To estimate the probability of a random velocity match, we query the NED database with 1,000 semi-random positions chosen one degree away in angular separation from a random NHICAT source position and set our random object's velocity at the velocity of the NHICAT source. Both position and velocity will be used to determine a match. Even though a velocity offset of 400 km s^{-1} appears very generous match criterion, we find that only 40 of our 1,000 semi-random sources were matched to objects within the NED database. Figure 8 compares the cumulative distributions of the match velocity difference for NOIRCAT (solid line) and for the randomly-matched sample (dashed line). As shown 99.8% of the NOIRCAT sample with unique optical/IR source identification have match velocity offsets below 200 km s^{-1} . The average velocity offset of the semi-random sample is 189 km s^{-1} .

For a conservative estimate of the number of random

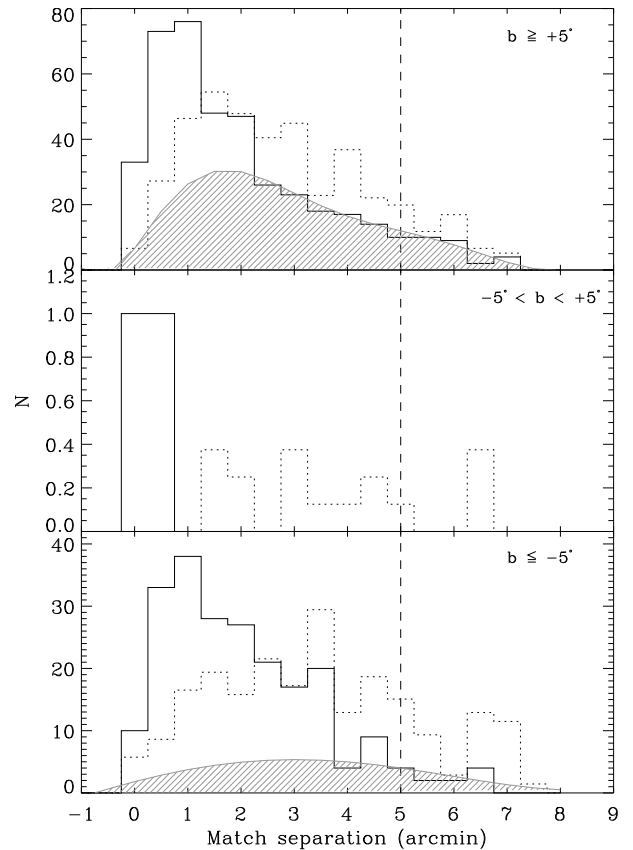


Figure 7. Distributions of match separations at three different Galactic latitude (b) ranges. See figure 6 for more details on the distributions marked by the black solid and the black dotted lines. The grey line-filled region shows the simulated random distribution scaled according to the tail end (at separations greater than five degrees) of the NOIRCAT match separation distribution. The vertical dashed line marks the match separation at five degrees in all three plots.

Table 5. Conservative estimate on the number of random matches which may have contributed to the final number of NOIRCAT matches *if* the NOIRCAT matching algorithm was solely based on the two-dimensional position of each object.

Region	Total NOIRCAT matches	Real	Random
$b \geq +5^\circ$	408	162	246
$-5^\circ < b < +5^\circ$	2	2	0
$b \leq -5^\circ$	215	161	54

matches within NOIRCAT, we now assume that the real velocity offset distribution does not have a tail and that all velocity offsets greater than 100 km s^{-1} can be attributed to a random velocity match. Similar to the previous test, we fit the tail-end (where velocity offsets are greater than 100 km s^{-1}) of the NOIRCAT velocity offset distribution with a scaled-down distribution of the semi-random sample. From this model of semi-random matches, we find that there is a 1.5% probability that the Flag 1, 2 and 5a NOIRCAT

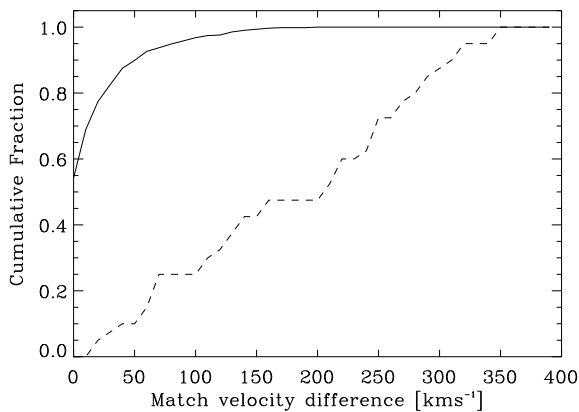


Figure 8. Normalised cumulative distribution of match velocity offsets for the NOIRCAT Flag 1, 2 and 5a sample (represented by the solid line) and the randomly-matched sample (represented by the dashed line).

sources may be due to random velocity matches. In summary, if we only used the source positions as a matching criteria then there is a 0.48 probability that a match is random. However, the inclusion of velocity as a match criteria significantly decreases the probability to 0.015 that a match made within NOIRCAT is spurious.

Although the positional accuracy is $3'$, we found 36 Flag 1 and 2 sources with match angular separations greater than $5.0'$. Of these, we found three with previous VLA observations listed in the NRAO Archive⁷. Figure 9 shows the VLA integrated flux contours overlaid on POSS II optical fields for these three NOIRCAT sources. These three sources (HIPASSJ1114+12, HIPASSJ1224+12 & HIPASSJ1243+13a) have match separations of $5.3'$, $6.1'$ and $6.3'$, respectively. García-Burillo et al. (2000) suggested that HIPASSJ1114+12's optical counterpart, NGC 3593, had accreted a gas-rich dwarf 1 Gyr ago and recent stars had time to form a central counter-rotating disk in the settling gas. For both HIPASSJ1224+12 and HIPASSJ1243+13a, the optical counterparts (NGC 4351 & NGC 4639) are part of the Virgo Cluster.

Using the MBSPECT tool of the MIRIAD data reduction package, we measure the total integrated flux (S_{INT}) and velocity width (W_{50}) from the VLA observations. As detailed in Table 6, the HIPASS integrated fluxes ($S_{\text{INT}}^{\text{HIPASS}}$) and the FWHM velocity widths (W_{50}^{HIPASS}) are very different to those measured from the VLA observations.

The HI total integrated flux observed by the VLA of HIPASSJ1114+12 is less than 1% of the total flux measured by HIPASS. Additionally, the HIPASS velocity width is five times greater than the velocity width detected by the VLA. This suggests that most of the HI emission measured by HIPASS in HIPASSJ1114+12 is diffuse and remains undetected by the VLA due to the lack of sensitivity at low column densities. This can also explain the difference in the

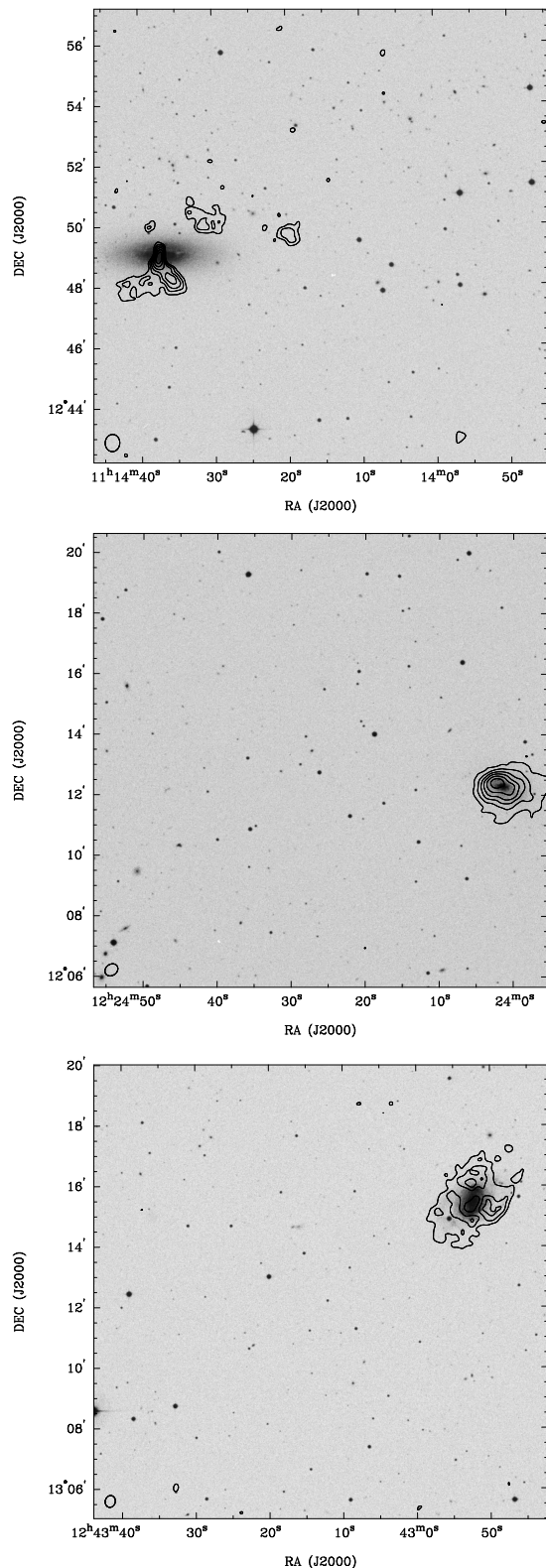


Figure 9. VLA integrated flux contours overlaid on POSSII images of 3 NOIRCAT sources with match separations greater than $5'$. The centre of the fields correspond to the HIPASS coordinate centres. From top to bottom: HIPASSJ1114+12 (NGC 3593), HIPASSJ1224+12 (NGC 4351) and HIPASSJ1243+13a (NGC 4639).

⁷ The National Radio Astronomy Observatory is a facility of the National Science Foundation operated under cooperative agreement by Associated Universities, Inc

Table 6. Properties of VLA observations of HIPASSJ1114+12, HIPASSJ1224+12 and HIPASSJ1243+13a.

HIPASS name	S_{INT} Jy km s ⁻¹	W_{50} km s ⁻¹	$S_{\text{INT}}^{\text{HIPASS}}$ Jy km s ⁻¹	W_{50}^{HIPASS} km s ⁻¹
J1114+12	0.43	44.0	14.1	215.1
J1224+12	8.79	210.3	5.3	109.3
J1243+13a	1.93	70.9	35.2	331.0

total integrated flux measured by HIPASS and the VLA of HIPASSJ1243+13a.

Conversely, the VLA has observed more HI integrated flux and a greater HI velocity width than HIPASS in HIPASSJ1224+12. Due to the strong radio emission from Virgo A (a Seyfert galaxy and a strong radio source), half of the emission profile was lost in the noise. Thus, we would expect that re-fitting the baseline would recover this flux. Figure 10 shows the HIPASS spectra of the three sources listed in Table 6.

4 SUMMARY

In this paper we have presented NOIRCAT, the optical/near-infrared counterpart catalogue to NHICAT. NOIRCAT contains optically-matched counterparts for 65% of the NHICAT sources. In combination with HOPCAT, NOIRCAT creates the largest catalogue of optical counterparts of HI sources, covering the entire sky in the declination range of $-90^\circ < \delta < +25.5^\circ$.

Of the 347 Flag 5 sources, 24.5% have optical counterparts with matching velocities in previously-published radio emission-line observations. Another 63.7% have probable optical counterparts to galaxies without published velocities (other than HIPASS observations). Although our estimates in Section 3 showed that more than half these matches should be real, only follow-up higher spatial resolution HI observations of these sources will help pinpoint the exact HI position and constrain the possible number of dark galaxies. Many of the Flag 5c sources lie in the direction of the Galactic plane and as such, are obscured behind our Galaxy.

Our statistical analysis indicated that up to 1.5% of the NOIRCAT matches may be due to random matches. It is not possible to determine the exact number of matches from the current sample as more observations at better sensitivities and higher resolution are required.

Ignoring the effects of mergers, Verde et al. (2002) postulated that a large fraction of low-mass halos ($< 10^9 M_\odot$) will be Toomre-stable and not form stars if the gas collapse during galaxy formation conserves angular momentum. In addition, simulations by Davies et al. (2006) predicted that ‘objects with scale sizes of tens of kpc and velocities of a few hundreds of km s⁻¹ can remain dark’. Contrary to these results, Taylor & Webster (2005) found that a majority of disks are predicted to be unstable and likely to form stars in at least half the hypothetical dark galaxies with baryon masses greater than $5 \times 10^6 M_\odot$. Standard reionisation models also propose that dark halos do not contain gas (Susa & Umemura 2004).

Although our statistical analysis with our current dataset

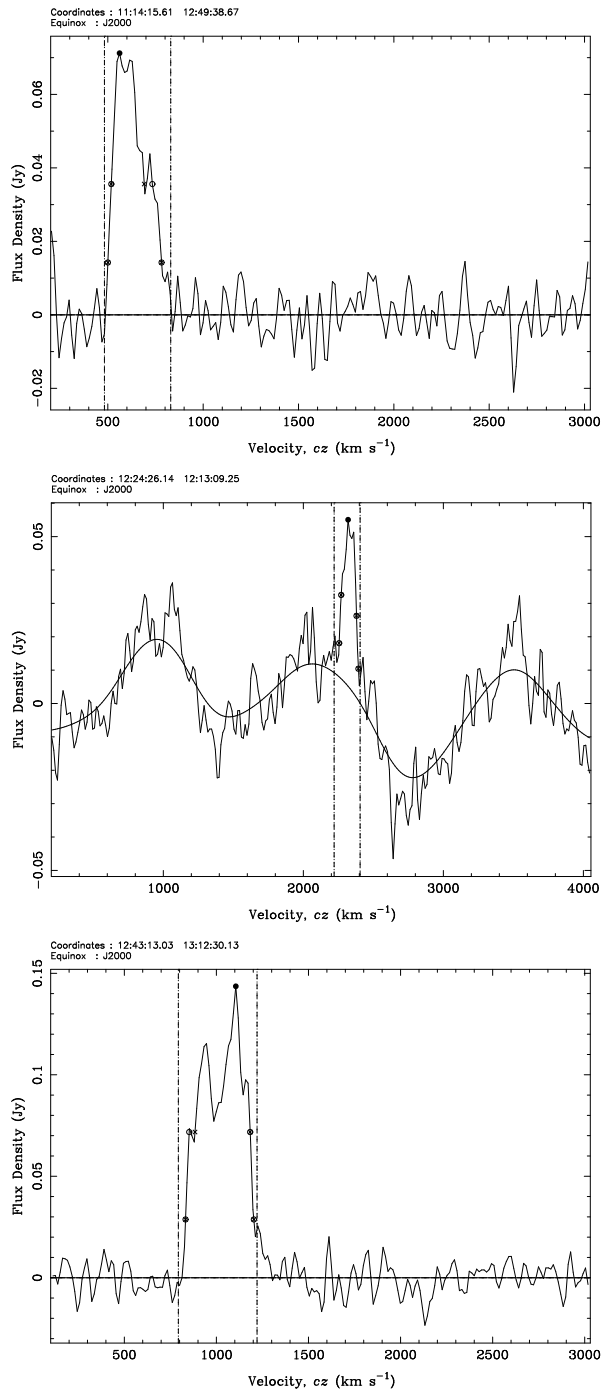


Figure 10. HIPASS spectrum of HIPASSJ1114+12 (top), HIPASSJ1224+12 (middle) and HIPASSJ1243+13a (bottom). The region between the dashed lines mark the HI emission profile and the solid line shows the fit to the baseline.

cannot confirm the number of possible dark galaxy candidates within NOIRCAT, detailed dark galaxy modelling by Taylor & Webster (2009) on the NHICAT completeness limits found that there could be ≈ 10 dark galaxies within NHICAT. These galaxies would be at the predicted limiting threshold for the formation of stars, if they formed. Hence, further observations of the Flag 5b and 5c sources may con-

firm the existence of these galaxies unless they are located in the direction of the Galactic plane.

As with other HIPASS catalogues, NOIRCAT will be publicly-available online at: (<http://hipass.aus-vo.org>). We will also submit NOIRCAT to the NED database. Sources classified as Flags 1, 2, 3, 4 and 5a are included in the official NOIRCAT online.

Acknowledgments. We thank the anonymous referee for providing detailed and constructive comments which greatly improved this paper. This research has made use of the NASA/IPAC Extragalactic Database (NED) which is operated by the Jet Propulsion Laboratory, California Institute of Technology, under contract with the National Aeronautics and Space Administration. This research has also made use of data products from the Two Micron All Sky Survey, which is a joint project of the University of Massachusetts and the Infrared Processing and Analysis Center/California Institute of Technology, funded by the National Aeronautics and Space Administration and the National Science Foundation. O.I.W. thanks Marianne Doyle and Mike Read for their help in acquiring the POSSII image fields as well as Stuart Wyithe for his comments and ideas about dark galaxies with respect to current reionisation models.

REFERENCES

- Barnes D. G., Staveley-Smith L., de Blok W. J. G., Oosterloo T., Stewart I. M., Wright A. E., Banks G. D., Bhathal R., et al. 2001, *MNRAS*, 322, 486
- Bell E. F., de Jong R. S., 2001, *ApJ*, 550, 212
- Bell E. F., McIntosh D. H., Katz N., Weinberg M. D., 2003, *ApJS*, 149, 289
- Bertin E., Arnouts S., 1996, *A&AS*, 117, 393
- Chengalur J. N., Giovanelli R., Haynes M. P., 1995, *AJ*, 109, 2415
- Davies J. I., Disney M. J., Minchin R. F., Auld R., Smith R., 2006, *MNRAS*, 368, 1479
- Disney M. J., 1976, *Nat*, 263, 573
- Doyle M. T., Drinkwater M. J., Rohde D. J., Pimblett K. A., Read M., Meyer M. J., Zwaan M. A., Ryan-Weber E., et al. 2005, *MNRAS*, 361, 34
- García-Burillo S., Sempere M. J., Combes F., Hunt L. K., Neri R., 2000, *A&A*, 363, 869
- Geller M. J., Kenyon S. J., Barton E. J., Jarrett T. H., Kewley L. J., 2006, *AJ*, 132, 2243
- Giovanelli R., Haynes M. P., 1989, *ApJ*, 346, L5
- Giuricin G., Biviano A., Girardi M., Mardirossian F., Mezzetti M., 1993, *A&A*, 275, 390
- Hanish D. J., Meurer G. R., Ferguson H. C., Zwaan M. A., Heckman T. M., Staveley-Smith L., Bland-Hawthorn J., Kilborn V. A., et al. 2006, *ApJ*, 649, 150
- Jansen R. A., Fabricant D., Franx M., Caldwell N., 2000a, *ApJS*, 126, 331
- Jansen R. A., Franx M., Fabricant D., Caldwell N., 2000b, *ApJS*, 126, 271
- Jarrett T., 2007, Masking of 2MASS images with nearby foreground stars, private communication
- Kilborn V. A., Forbes D. A., Koribalski B. S., Brough S., Kern K., 2006, *MNRAS*, 371, 739
- Kilborn V. A., Staveley-Smith L., Marquarding M., Webster R. L., Malin D. F., Banks G. D., Bhathal R., de Blok W. J. G., et al. 2000, *AJ*, 120, 1342
- Kilborn V. A., Webster R. L., Staveley-Smith L., Marquarding M., Banks G. D., Barnes D. G., Bhathal R., de Blok W. J. G., Boyce P. J., et al. 2002, *AJ*, 124, 690
- Klypin A., Gottlöber S., Kravtsov A. V., Khokhlov A. M., 1999, *ApJ*, 516, 530
- Koribalski B. S., Staveley-Smith L., Kilborn V. A., Ryder S. D., Kraan-Korteweg R. C., Ryan-Weber E. V., Ekers R. D., Jerjen H., et al. 2004, *AJ*, 128, 16
- Meurer G. R., Carignan C., Beaulieu S. F., Freeman K. C., 1996, *AJ*, 111, 1551
- Meyer M. J., Zwaan M. A., Webster R. L., Staveley-Smith L., Ryan-Weber E., Drinkwater M. J., Barnes D. G., Howlett M., et al. 2004, *MNRAS*, 350, 1195(MZ04)
- Moore B., Ghigna S., Governato F., Lake G., Quinn T., Stadel J., Tozzi P., 1999, *ApJ*, 524, L19
- Reid I. N., Brewer C., Brucato R. J., McKinley W. R., Maury A., Mendenhall D., Mould J. R., Mueller J., et al. 1991, *PASP*, 103, 661
- Roberts M. S., 1962, *AJ*, 67, 437
- Ryan-Weber E., Koribalski B. S., Staveley-Smith L., Jerjen H., Kraan-Korteweg R. C., Ryder S. D., Barnes D. G., de Blok W. J. G., et al. 2002, *AJ*, 124, 1954
- Ryder S. D., Koribalski B., Staveley-Smith L., Kilborn V. A., Malin D. F., Banks G. D., Barnes D. G., Bhathal R., et al. 2001, *ApJ*, 555, 232
- Schneider S. E., 1996, in Skillman E. D., ed., *ASP Conf. Ser. 106: The Minnesota Lectures on Extragalactic Neutral Hydrogen HI Selection Effects and the Galaxy Mass Function*. pp 323–+
- Schneider S. E., Helou G., Salpeter E. E., Terzian Y., 1983, *ApJ*, 273, L1
- Susa H., Umemura M., 2004, *ApJ*, 610, L5
- Taylor E. N., Webster R. L., 2005, *ApJ*, 634, 1067
- Taylor E. N., Webster R. L., 2009, On star formation and the existence of dark galaxies, in preparation
- Turner N. J. J., MacFadyen A., 1997, *MNRAS*, 285, 125
- Verde L., Oh S. P., Jimenez R., 2002, *MNRAS*, 336, 541
- Wong O. I., Ryan-Weber E. V., Garcia-Appadoo D. A., Webster R. L., Staveley-Smith L., Zwaan M. A., Meyer M. J., Barnes D. G., et al. 2006, *MNRAS*, pp 911–+

APPENDIX A: NHICAT PROPERTIES OF 221 FLAG 5B SOURCES FOR WHICH NED HAD 1 OR MORE SOURCES WHICH WERE CLASSIFIED AS GALAXIES WITH POSITIONAL MATCHES ONLY

This paper has been typeset from a \TeX / \LaTeX file prepared by the author.

Table A1. NHICAT properties of 219 Flag 5b sources for which NED had 1 or more sources which were classified as galaxies with positional matches only .

HIPASS_name	RA_HIPASS (J2000)	Dec_HIPASS (J2000)	Vel_HIPASS (km s ⁻¹)	W_HIPASS (km s ⁻¹)
HIPASSJ0003+08	00:03:14.6	08:42:34	2626.7	139.1
HIPASSJ0003+15	00:03:58.4	15:11:59	873.8	100.6
HIPASSJ0010+13	00:10:42.8	13:43:57	1740.5	76.4
HIPASSJ0014+07	00:14:39.8	07:30:58	3513.9	108.2
HIPASSJ0016+07	00:16:54.8	07:12:06	3967.5	402.3
HIPASSJ0017+04	00:17:01.1	04:55:42	6528.2	501.3
HIPASSJ0019+04	00:19:28.3	04:04:42	3023.8	543.1
HIPASSJ0020+08	00:20:06.4	08:28:58	5604.5	67.0
HIPASSJ0020+10	00:20:03.0	10:53:16	1142.4	134.3
HIPASSJ0021+08	00:21:00.9	08:35:06	693.1	41.3
HIPASSJ0028+11	00:28:54.3	11:18:15	6207.9	81.3
HIPASSJ0033+02	00:33:44.3	02:40:37	4389.2	225.9
HIPASSJ0109+13	01:09:57.9	13:18:37	4219.4	166.5
HIPASSJ0120+05	01:20:20.7	05:49:57	2165.0	82.8
HIPASSJ0121+12	01:21:20.6	12:25:35	642.7	119.1
HIPASSJ0129+10	01:29:33.0	10:00:01	9530.9	93.3
HIPASSJ0131+23	01:31:21.7	23:54:22	3413.0	61.5
HIPASSJ0133+14	01:33:13.0	14:23:11	671.0	78.0
HIPASSJ0134+04	01:34:53.5	04:24:17	1959.5	108.1
HIPASSJ0142+02	01:42:28.4	02:56:20	1763.9	80.6
HIPASSJ0143+19	01:43:15.9	19:58:20	496.7	71.7
HIPASSJ0158+04	01:58:05.1	04:21:43	4765.3	312.4
HIPASSJ0210+06	02:10:41.4	06:46:27	1604.0	103.3
HIPASSJ0211+14	02:11:49.9	14:11:42	3812.7	58.9
HIPASSJ0221+14	02:21:52.1	14:19:27	3586.3	51.7
HIPASSJ0237+12	02:37:26.3	12:31:07	960.2	50.9
HIPASSJ0239+12	02:39:29.9	12:41:25	3554.1	154.2
HIPASSJ0243+16	02:43:16.8	16:45:37	821.4	44.8
HIPASSJ0247+03	02:47:55.9	03:53:38	1024.6	90.5
HIPASSJ0250+03	02:50:56.6	03:22:08	3009.1	46.5
HIPASSJ0251+06	02:51:32.0	06:02:30	6921.3	111.5
HIPASSJ0253+02	02:53:48.6	02:20:42	6731.0	349.4
HIPASSJ0253+06	02:53:09.3	06:32:03	5431.5	328.9
HIPASSJ0314+24	03:14:22.0	24:10:20	1303.8	143.9
HIPASSJ0320+17	03:20:24.3	17:18:56	355.2	74.2
HIPASSJ0332+15	03:32:18.4	15:26:35	6141.0	123.1
HIPASSJ0339+08	03:39:33.5	08:31:37	6728.9	110.3
HIPASSJ0340+05	03:40:51.5	05:22:08	6137.2	65.2
HIPASSJ0341+24	03:41:19.2	24:00:54	1259.6	110.3
HIPASSJ0341+18	03:41:53.5	18:07:21	1296.8	45.3
HIPASSJ0345+08	03:45:11.7	08:51:12	1755.6	40.9
HIPASSJ0345+02	03:45:36.6	02:12:00	4256.7	75.1
HIPASSJ0354+06	03:54:41.4	06:37:15	3470.4	249.8
HIPASSJ0413+24	04:13:29.7	24:50:23	3877.4	130.3
HIPASSJ0414+02	04:14:24.5	02:46:54	3336.4	270.8
HIPASSJ0415+02	04:15:41.3	02:28:45	3584.6	140.6
HIPASSJ0417+13	04:17:55.1	13:30:32	7510.4	396.3
HIPASSJ0421+10	04:21:10.1	10:09:26	7694.7	93.6
HIPASSJ0428+18	04:28:50.7	18:57:19	4793.7	87.5
HIPASSJ0431+07	04:31:07.3	07:24:28	3917.2	104.9
HIPASSJ0432+16	04:32:42.8	16:12:18	4107.1	44.6
HIPASSJ0446+08	04:46:31.4	08:18:58	4651.7	241.8
HIPASSJ0503+18	05:03:14.4	18:24:56	5005.8	389.1
HIPASSJ0506+25	05:06:50.7	25:12:46	3059.7	254.5
HIPASSJ0508+10	05:08:49.5	10:45:00	1669.1	555.1
HIPASSJ0519+22	05:19:44.1	22:56:38	7182.5	314.9
HIPASSJ0520+17	05:20:50.9	17:02:24	6621.8	168.8
HIPASSJ0524+04	05:24:58.6	04:31:11	519.3	166.5
HIPASSJ0524+07	05:24:18.8	07:23:46	4395.3	106.7
HIPASSJ0527+15	05:27:42.9	15:52:52	5598.2	161.2
HIPASSJ0531+08	05:31:05.6	08:20:12	961.0	90.1

Table A1 – continued

HIPASS_name	RA_HIPASS (J2000)	Dec_HIPASS (J2000)	Vel_HIPASS (km s ⁻¹)	W_HIPASS (km s ⁻¹)
HIPASSJ0544+04	05:44:24.9	04:13:03	3537.2	66.7
HIPASSJ0545+05	05:45:02.0	05:04:09	387.8	122.0
HIPASSJ0547+17	05:47:07.9	17:35:07	5571.2	90.9
HIPASSJ0554+18	05:54:10.1	18:00:42	5726.2	46.7
HIPASSJ0556+13	05:56:26.8	13:40:07	7877.4	264.9
HIPASSJ0559+15	05:59:53.0	15:36:00	5454.9	196.8
HIPASSJ0603+08	06:03:49.3	08:38:43	5380.5	206.6
HIPASSJ0605+19	06:05:26.6	19:29:32	5763.3	286.2
HIPASSJ0620+20	06:20:36.1	20:10:49	1318.0	138.1
HIPASSJ0621+11	06:21:18.5	11:06:52	5602.4	195.6
HIPASSJ0622+11	06:22:49.2	11:08:28	5509.4	384.1
HIPASSJ0623+04	06:23:52.1	04:16:55	2867.8	102.5
HIPASSJ0624+23	06:24:35.3	23:21:20	1464.1	72.8
HIPASSJ0626+24	06:26:39.8	24:40:18	1473.2	99.2
HIPASSJ0630+23	06:30:04.1	23:34:08	1452.4	135.4
HIPASSJ0630+08	06:30:09.2	08:21:16	363.7	53.4
HIPASSJ0630+16	06:30:08.5	16:47:50	2526.4	275.1
HIPASSJ0631+02	06:31:12.9	02:44:05	2774.1	114.7
HIPASSJ0633+21	06:33:12.5	21:02:15	5451.5	467.6
HIPASSJ0635+20	06:35:32.9	20:36:31	4329.3	269.4
HIPASSJ0635+11	06:35:47.6	11:13:11	3575.4	76.6
HIPASSJ0635+14	06:35:52.7	14:36:39	4023.3	347.5
HIPASSJ0637+03	06:37:39.3	03:24:50	3428.5	159.8
HIPASSJ0637+22	06:37:56.1	22:39:24	1380.5	114.0
HIPASSJ0645+22	06:45:42.5	22:25:58	4482.1	195.0
HIPASSJ0656+06b	06:56:27.1	06:14:42	6783.4	228.5
HIPASSJ0704+13	07:04:55.2	13:56:18	2367.5	53.1
HIPASSJ0705+02	07:05:43.6	02:37:12	1744.6	46.3
HIPASSJ0710+05	07:10:09.9	05:16:33	3609.1	139.6
HIPASSJ0714+06	07:14:00.6	06:18:00	8422.1	139.7
HIPASSJ0730+07	07:30:02.3	07:14:41	3920.0	94.0
HIPASSJ0731+08	07:31:16.0	08:00:01	1882.9	55.2
HIPASSJ0755+03	07:55:52.3	03:27:05	9720.8	93.4
HIPASSJ0818+04	08:18:14.2	04:37:29	4221.7	52.2
HIPASSJ0831+07	08:31:31.0	07:00:18	1850.8	128.2
HIPASSJ0901+21	09:01:20.5	21:13:10	7641.6	86.5
HIPASSJ0905+21	09:05:26.9	21:38:58	3073.6	107.0
HIPASSJ0908+05a	09:08:12.9	05:55:02	1313.7	71.4
HIPASSJ0922+03	09:22:25.6	03:51:36	4139.3	128.9
HIPASSJ0942+04	09:42:46.9	04:49:53	1955.0	66.2
HIPASSJ1003+11	10:03:15.9	11:29:33	3501.6	52.8
HIPASSJ1027+24	10:27:07.6	24:10:09	1211.8	52.5
HIPASSJ1031+25	10:31:34.9	25:16:07	1282.3	125.4
HIPASSJ1034+23	10:34:38.9	23:03:06	1238.0	49.3
HIPASSJ1052+07	10:52:59.4	07:37:52	3392.0	80.2
HIPASSJ1106+19	11:06:02.6	19:49:15	1334.9	38.3
HIPASSJ1113+21	11:13:43.0	21:34:37	1440.2	164.6
HIPASSJ1119+03	11:19:10.4	03:36:02	7169.7	202.7
HIPASSJ1119+09	11:19:16.4	09:34:56	995.2	69.9
HIPASSJ1122+13	11:22:33.2	13:40:32	896.3	51.4
HIPASSJ1129+11	11:29:44.4	11:58:38	3240.9	94.6
HIPASSJ1130+23	11:30:48.2	23:05:26	2912.0	179.8
HIPASSJ1137+18	11:37:29.7	18:22:18	946.0	41.1
HIPASSJ1148+23	11:48:55.2	23:48:54	528.2	101.1
HIPASSJ1204+16	12:04:00.7	16:30:43	2063.9	173.6
HIPASSJ1205+21	12:05:10.1	21:29:07	3128.5	37.3
HIPASSJ1209+14	12:09:56.3	14:20:57	820.0	52.6
HIPASSJ1213+16	12:13:03.1	16:11:21	7135.9	83.5
HIPASSJ1214+09	12:14:41.5	09:11:45	1784.3	121.9
HIPASSJ1215+09b	12:15:53.0	09:40:01	2219.4	35.6
HIPASSJ1215+12	12:15:26.5	12:59:54	2090.3	36.0
HIPASSJ1218+07	12:18:23.0	07:39:09	3956.6	150.4
HIPASSJ1219+06b	12:19:53.6	06:39:42	480.7	41.5

Table A1 – *continued*

HIPASS_name	RA_HIPASS (J2000)	Dec_HIPASS (J2000)	Vel_HIPASS (km s ⁻¹)	W_HIPASS (km s ⁻¹)
HIPASSJ1230+09	12:30:22.3	09:31:28	495.9	69.5
HIPASSJ1230+17	12:30:06.6	17:24:52	2556.1	282.9
HIPASSJ1231+20	12:31:44.5	20:23:28	1332.1	68.6
HIPASSJ1234+15	12:34:41.7	15:12:11	671.1	91.2
HIPASSJ1240+13	12:40:01.5	13:50:48	1004.3	40.2
HIPASSJ1242+05	12:42:43.3	05:46:12	989.1	106.0
HIPASSJ1243+07	12:43:13.1	07:37:56	1314.7	66.8
HIPASSJ1244+12	12:44:07.0	12:08:52	1008.1	111.7
HIPASSJ1250+17	12:50:22.7	17:30:18	843.5	116.9
HIPASSJ1256+19	12:56:04.9	19:07:38	418.4	33.0
HIPASSJ1314+23	13:14:11.2	23:11:30	3441.9	76.6
HIPASSJ1327+10	13:27:18.7	10:03:17	1050.0	50.8
HIPASSJ1336+08	13:36:04.2	08:51:39	1159.4	130.8
HIPASSJ1355+17	13:55:22.9	17:47:24	956.7	97.5
HIPASSJ1403+09	14:03:21.3	09:25:34	4638.5	43.9
HIPASSJ1404+08a	14:04:15.4	08:47:43	6289.2	55.2
HIPASSJ1406+22	14:06:56.0	22:04:40	2320.0	122.3
HIPASSJ1415+16	14:15:38.2	16:32:48	2270.6	90.0
HIPASSJ1420+08	14:20:54.4	08:40:24	1298.0	81.9
HIPASSJ1435+05	14:35:24.0	05:17:26	1636.3	96.0
HIPASSJ1435+13	14:35:37.9	13:02:19	1827.0	227.9
HIPASSJ1436+21	14:36:36.3	21:02:51	5458.5	291.9
HIPASSJ1445+07	14:45:16.0	07:52:49	1690.6	38.3
HIPASSJ1526+14	15:26:22.1	14:25:11	8694.9	136.8
HIPASSJ1538+12a	15:38:18.2	12:58:47	1860.5	158.2
HIPASSJ1545+12	15:45:42.6	12:30:40	1122.5	110.4
HIPASSJ1548+16	15:48:58.1	16:43:14	2051.9	94.5
HIPASSJ1557+14	15:57:56.1	14:58:41	11276.2	62.4
HIPASSJ1604+14	16:04:10.8	14:37:54	4793.0	111.5
HIPASSJ1606+08	16:06:14.9	08:29:46	1362.9	145.9
HIPASSJ1614+02	16:14:14.1	02:30:46	4852.8	78.3
HIPASSJ1621+20	16:21:38.7	20:52:25	3100.6	128.1
HIPASSJ1735+02	17:35:34.7	02:46:46	10311.9	139.3
HIPASSJ1736+15	17:36:49.7	15:12:00	6613.4	45.2
HIPASSJ1747+04	17:47:06.5	04:11:58	8158.7	80.9
HIPASSJ1747+18	17:47:31.8	18:18:00	5827.3	57.7
HIPASSJ1750+21	17:50:13.4	21:15:50	3221.7	82.4
HIPASSJ1752+22	17:52:56.0	22:54:44	8255.3	143.2
HIPASSJ1754+02	17:54:40.9	02:55:07	1761.7	187.1
HIPASSJ1758+14	17:58:46.7	14:47:43	2957.5	133.8
HIPASSJ1804+21	18:04:37.7	21:39:04	2224.0	196.6
HIPASSJ1805+17	18:05:05.9	17:19:09	5548.3	149.7
HIPASSJ1805+23a	18:05:31.2	23:13:00	2339.6	101.4
HIPASSJ1805+23b	18:05:57.2	23:26:38	6666.8	58.6
HIPASSJ1807+09	18:07:57.2	09:46:19	2070.0	150.5
HIPASSJ1807+25	18:07:22.0	25:19:41	4688.0	126.2
HIPASSJ1817+14	18:17:07.7	14:25:02	5362.7	200.5
HIPASSJ1819+14	18:19:56.8	14:40:45	5181.1	132.5
HIPASSJ1828+06	18:28:49.8	06:32:26	2957.3	158.5
HIPASSJ1832+06	18:32:12.6	06:25:06	2823.3	90.6
HIPASSJ1833+10	18:33:29.4	10:38:48	3165.1	158.1
HIPASSJ1837+11	18:37:37.3	11:55:17	3584.4	80.9
HIPASSJ1837+22	18:37:45.3	22:04:32	4101.0	132.2
HIPASSJ1839+13	18:39:35.3	13:19:21	3892.9	151.4
HIPASSJ1842+17	18:42:53.8	17:02:14	3909.8	89.4
HIPASSJ1842+15	18:42:58.3	15:00:29	4263.6	36.6
HIPASSJ1843+19	18:43:27.2	19:26:41	4300.7	206.1
HIPASSJ1846+22	18:46:11.3	22:36:24	4698.6	316.5
HIPASSJ1849+18	18:49:55.0	18:44:16	3081.8	130.0
HIPASSJ1912+13	19:12:37.3	13:23:54	2776.7	112.2
HIPASSJ1915+20	19:15:00.4	20:11:43	4710.3	545.6
HIPASSJ1917+04	19:17:39.1	04:27:21	6182.8	167.2

Table A1 – continued

HIPASS_name	RA_HIPASS (J2000)	Dec_HIPASS (J2000)	Vel_HIPASS (km s ⁻¹)	W_HIPASS (km s ⁻¹)
HIPASSJ1950+18b	19:50:52.8	18:23:51	3979.2	310.9
HIPASSJ2004+07	20:04:12.1	07:23:37	5943.3	145.0
HIPASSJ2004+14	20:04:46.0	14:06:19	4406.0	138.4
HIPASSJ2015+12	20:15:50.3	12:40:44	1950.9	51.6
HIPASSJ2042+07	20:42:16.7	07:36:53	5737.4	120.5
HIPASSJ2045+12	20:45:19.4	12:53:03	4916.0	124.2
HIPASSJ2109+21	21:09:41.2	21:18:16	3394.7	111.2
HIPASSJ2112+12	21:12:26.7	12:37:20	4857.6	200.0
HIPASSJ2132+07	21:32:52.3	07:58:22	3490.8	66.7
HIPASSJ2142+22	21:42:27.7	22:38:58	5623.0	84.4
HIPASSJ2149+14	21:49:34.4	14:14:35	1103.0	119.4
HIPASSJ2158+14	21:58:34.9	14:07:01	1703.2	90.5
HIPASSJ2207+15	22:07:06.0	15:59:05	1767.1	64.3
HIPASSJ2208+03	22:08:05.5	03:36:27	4012.2	152.7
HIPASSJ2209+01	22:09:44.7	01:59:07	3840.3	100.7
HIPASSJ2211+17	22:11:54.7	17:54:35	1738.0	151.3
HIPASSJ2224+22	22:24:52.1	22:58:23	1249.8	90.6
HIPASSJ2225+06	22:25:31.1	06:23:15	8377.6	69.1
HIPASSJ2251+07	22:51:29.7	07:15:58	3211.6	105.6
HIPASSJ2253+11	22:53:48.0	11:16:15	2243.5	148.8
HIPASSJ2255+11	22:55:37.8	11:03:54	2064.3	146.8
HIPASSJ2301+12	23:01:06.0	12:44:53	2805.2	213.5
HIPASSJ2308+17	23:08:47.5	17:12:44	1764.2	142.0
HIPASSJ2316+05	23:16:00.0	05:11:47	9884.7	152.9
HIPASSJ2319+16	23:19:36.8	16:06:43	7222.5	478.0
HIPASSJ2322+13	23:22:27.2	13:52:11	7799.7	64.1
HIPASSJ2333+04	23:33:20.8	04:23:33	5814.1	88.9
HIPASSJ2336+12	23:36:29.9	12:46:22	6184.4	62.1
HIPASSJ2336+14	23:36:41.6	14:12:05	3971.0	174.2
HIPASSJ2339+07	23:39:32.7	07:48:53	3430.9	60.5
HIPASSJ2349+02	23:49:53.6	02:43:12	5307.8	222.8
HIPASSJ2353+07	23:53:55.1	07:56:25	5132.9	167.3
HIPASSJ2357+23	23:57:57.2	23:59:54	10927.8	100.2
HIPASSJ2358+04	23:58:15.2	04:47:37	3035.2	110.7
HIPASSJ2359+02	23:59:17.3	02:42:05	2616.0	147.8